© 2022. Published by The Company of Biologists Ltd | Development (2022) 149, dev200729. doi:10.1242/dev.200729

RESEARCH REPORT

Brain vascular damage-induced lymphatic ingrowth is directed by Cxcl12b/Cxcr4a

Jingying Chen[1,2], Jianbo He[1] and Lingfei Luo[1,2,*]

ABSTRACT

After ischemic stroke, promotion of vascular regeneration without causing uncontrolled vessel growth appears to be the major challenge for pro-angiogenic therapies. The molecular mechanisms underlying how nascent blood vessels (BVs) are correctly guided into the post-ischemic infarction area remain unknown. Here, using a zebrafish cerebrovascular injury model, we show that chemokine signaling provides crucial guidance cues to determine the growing direction of ingrown lymphatic vessels (iLVs) and, in turn, that of nascent BVs. The chemokine receptor Cxcr4a is transcriptionally activated in the iLVs after injury, whereas its ligand Cxcl12b is expressed in the residual central BVs, the destinations of iLV ingrowth. Mutant and mosaic studies indicate that Cxcl12b/Cxcr4a-mediated chemotaxis is necessary and sufficient to determine the growing direction of iLVs and nascent BVs. This study provides a molecular basis for how the vessel directionality of cerebrovascular regeneration is properly determined, suggesting potential application of Cxcl12b/Cxcr4a in the development of post-ischemic pro-angiogenic therapies.

KEY WORDS: Chemokine, Zebrafish, Cerebrovascular regeneration, Ingrown lymphatic vessels, Growth direction

INTRODUCTION

After ischemic stroke, the formation of nascent blood vessels (BVs) by neoangiogenesis participates in the functional recovery of injured tissues. The promotion of directional neoangiogenesis without causing uncontrolled vessel growth turns out to be one of the major challenges for pro-angiogenic therapies (Grunewald et al., 2006; Navaratna et al., 2009). The nascent BVs must be induced and correctly directed to revascularize the injured parenchyma, but not the uninjured regions. An understanding of cellular and molecular mechanisms underlying directional neoangiogenesis will help identify therapeutic targets for ischemic brain diseases (Liu et al., 2014).

Recent evidence suggests that chemokines are capable of regulating angiogenesis by recruiting leukocytes and endothelial progenitor cells (EPCs). For example, during hypoxia, the chemokine CXCL12 is upregulated by hypoxia induced factor 1α (HIF1α) and binds to the G-protein coupled CXC family chemokine receptor CXCR4, which is expressed in EPCs and associates with homing of EPCs to the site of injury to promote angiogenesis (Jin et al., 2006; Petit et al., 2007; Wang et al., 2012). More evidence supporting roles of CXCL12/CXCR4 in angiogenesis come from observations that the peripheral neurons expressing CXCL12 control nerve vessel alignment over a distance (Li et al., 2013) and Cxcr4 is required for arterial morphogenesis in the zebrafish embryo and fin regeneration (Bussmann et al., 2011; Fujita et al., 2011; Siekmann et al., 2009; Xu et al., 2014). Furthermore, chemokine signaling directs trunk lymphangiogenesis along the preexisting intersegmental blood vessels (Bussmann et al., 2010; Cha et al., 2012; Peng et al., 2022) and guides coronary vascular formation to support later lymphatic development and heart regeneration (Harrison et al., 2015, 2019; Gancz et al., 2019). However, although these studies have shown that chemokine signaling is crucial for angiogenesis and lymphangiogenesis, it remains unclear whether it plays any role in the guidance of neoangiogenesis to re-vascularize the injured brain parenchyma.

Recently, meningeal lymphatic vessels (mLVs) have been discovered in mammals and zebrafish to drain interstitial fluid from brain (Aspelund et al., 2015; Louveau et al., 2015; Castranova et al., 2021). Unlike the mLVs located in the dura mater, non-lumenized brain lymphatic endothelial cells (BLECs/muLECs/FGPs in zebrafish) and leptomeningeal lymphatic endothelial cells (LLECs in mouse) locate within the meningeal layer (Bower et al., 2017; Venero Galanternik et al., 2017; van Lessen et al., 2017; Shibata-Germanos et al., 2019). The zebrafish model system has substantially contributed to the understanding of cellular and molecular mechanisms underlying brain vascular regeneration (Liu et al., 2016; Chen et al., 2019, 2021). After cerebrovascular injury, the non-lumenized BLECs rapidly ingrow into the injured parenchyma to form lumenized ingrown lymphatic vessels (iLVs). The iLVs can be subdivided into standalone iLVs and track iLVs. The former transdifferentiate into early-regenerated BVs, whereas the latter acts as 'growing tracks' to support and guide the growth of late-regenerated BVs (Chen et al., 2019, 2021). These studies indicate that the growing direction of nascent BVs is determined by the preformed iLVs, regardless of whether they are standalone iLVs or track iLVs. However, mechanisms for how the iLVs are properly directed into the injured area remain unknown. In this study, we have found that the chemokine receptor Cxcr4a is transcriptionally activated in the ingrown lymphatic endothelial cells (iLECs) in response to brain vascular injury, whereas its ligand Cxcl12b is expressed in the residual central BVs, which turn out to be the destinations of iLV ingrowth. Furthermore, mutant and mosaic studies indicate that Cxcl12b/Cxcr4a-mediated chemotaxis is necessary and sufficient to direct the ingrowth of iLVs and in turn the growing direction of nascent BVs. In conclusion, after brain vascular injury, Cxcl12b/Cxcr4a become active to control the direction of lymphangiogenesis and cerebrovascular regeneration, thus avoiding uncontrolled vessel growth.

[1]Institute of Developmental Biology and Regenerative Medicine, Southwest University, Beibei, 400715 Chongqing, China. [2]University of Chinese Academy of Sciences (Chongqing), Chongqing Institute of Green and Intelligent Technology, Chinese Academy of Sciences, Beibei, 400714 Chongqing, China.

*Author for correspondence (lluo@swu.edu.cn)

J.C., 0000-0001-7852-6457; L.L., 0000-0002-5318-8137

Handling Editor: Ken Poss
Received 6 March 2022; Accepted 6 June 2022

Development (2022) 149, dev200729. doi:10.1242/dev.200729

RESULTS AND DISCUSSION

Cxcr4a is transcriptionally activated in the iLECs

To gain insight into the directionality of vessel growth during brain vascular regeneration, the zebrafish NTR-Mtz cerebrovascular injury model was applied (Chen et al., 2019). Under the *Tg(lyve1b:DsRed; kdrl:DenNTR)* transgenic background in which the blood endothelial cells (BECs) and brain lymphatic endothelial cells (LECs) were labeled by the *kdrl* and *lyve1b* promoter-driven fluorophores (Okuda et al., 2012), respectively, live imaging from 1.5 days post Mtz treatment (dpt) illustrated that the *lyve1b*+ iLVs presented regular growing directions. In most cases, the iLVs migrated with clear directionality from choroidal vascular plexus (CVP) to basal communicating artery (BCA) in the midbrain, and from primordial hindbrain channel (PHBC) to basilar artery (BA) in the hindbrain (Isogai et al., 2001) (Fig. 1A-C; Movie 1). These ingrowing directions of iLVs were confirmed by the *fli1+kdrl*− vessels under the *Tg(fli1:GFP; kdrl:mCherry; kdrl:DenNTR)* transgenic background (Fig. S1; Movie 2), in which both BECs and LECs were labeled by *fli1* (Yaniv et al., 2006; Küchler et al., 2006). These data indicate that the ingrowth of iLVs in response to cerebrovascular injury exhibits regular directionality.

To investigate mechanisms that determine the growing direction of iLVs, we first analyzed the expressions of chemokine receptors and ligands after cerebrovascular injury. The Cxcr4a+ vessels were detected in the injured brain under the *Tg(cxcr4a^{BAC}:RFP; kdrl:DenNTR)* transgenic background (Fig. S2A-C), in which TagRFP-T was driven by a bacterial artificial chromosome (BAC) sequence including the *cxcr4a* promoter-enhancer region (Cha et al., 2012). Under the *Tg(lyve1b:GFP; kdrl:DenNTR)* transgenic background, in contrast to the absence of FISH-*cxcr4a* signal in the BLECs and BVs of uninjured brain (Fig. 1D), the majority of *cxcr4a* was activated in the endothelial cells at the central brain including the leading iLECs (arrowheads, Fig. 1E,F), but less or even absent in the peripheral LECs (arrows, Fig. 1E). This expression of *cxcr4a* in the iLECs was validated by co-labeling of FISH-*cxcr4a* or *cxcr4a^{BAC}:RFP* transgene with *prox1a:KalTA4;UAS:TagRFP* transgene, *lyve1b:DsRed* transgene, FISH-*vegfr3* (also known as *flt4*) and anti-Prox1 antibodies (Fig. S2D-P). Moreover, RT-PCR using sorted LECs from the brain showed significant upregulation of *cxcr4a* after injury (Fig. S2Q). These data demonstrate the transcriptional activation of *cxcr4a* in response to the cerebrovascular injury, mainly in the iLECs.

Cxcl12b is expressed in the destinations of iLV ingrowth

Given the transcriptional activation of the chemokine receptor Cxcr4a in the iLECs, the expression of its ligand Cxcl12b was analyzed after cerebrovascular injury. The uninjured brain was devoid of *cxcl12b* expression (Fig. 1G), which remained at low levels at 1 dpt after Mtz injury (Fig. 1H,J). However, transcriptional activation of *cxcl12b* became apparent in the residual central BVs including BCA, BA, posterior communicating segment (PCS) and anterior mesencephalic central artery (AMCtA) at 1.5 dpt, maintained at 2.5 dpt and terminated at 3.5 dpt (Fig. 1H-K). Application of the mural cell-labeling transgene *abcc9^{BAC}:Gal4FF; UAS:EGFP* (Ando et al., 2019) indicated that the *cxcl12b* transcripts were accumulated in the *kdrl*+ BECs, but not the *abcc9*+ mural cells (Fig. 1H,I; Fig. S3). The comparison of *cxcl12b* patterns (Fig. 1H) with Cxcr4a patterns (Fig. 1E; Fig. S2C) and iLV ingrowth from 1.5 dpt (Fig. 1B; Movie 1) revealed their spatial and temporal correlations. Spatially, the *cxcl12b* expression was localized in the residual central blood endothelia, which were exactly the destinations of iLV ingrowth (Fig. 1L-N). Temporally, the timing of *cxcl12b* expression (Fig. 1H-J), which was active from 1.5 dpt to 2.5 dpt, was consistent with the timing of iLV lymphangiogenesis (Fig. 1B; Movie 1). These data indicate transcriptional activation of *cxcl12b* in the residual central blood endothelia, the destinations of iLV ingrowth.

Cxcr4a/Cxcl12b is required and sufficient for determining the directionality of iLV ingrowth

Both track iLVs and standalone iLVs of injured brain in sibling migrated with peripheral-to-medial directionality (Fig. 2A, in blue and purple dashed boxes). To investigate whether Cxcr4a/Cxcl12b is required for the directionality of iLV ingrowth, we examined the post-injured lymphangiogenesis and vascular regeneration in the *cxcr4a* and *cxcl12b* mutants (Bussmann et al., 2011). From 2 dpt to 4 dpt, the iLV ingrowth and cerebrovascular regeneration still occurred in the *cxcr4a* mutant (Fig. 2A,B,D). However, the vessels lost their peripheral-to-medial directionality and exhibited more iLV and BV branch points in the mutants (Fig. 2F). The number of iLVs ingrowth from CVP to BCA and from PHBC to BA (from peripheral to medial) was significantly reduced (Fig. 2G). Consequently, the majority of nascent BV connections between middle mesencephalic central arteries (MMCtAs) and BCA (Fig. 2A,B, arrows to asterisks) as well as between central artery (CtA) and BA (Fig. S4A,B, asterisks) failed to form in the *cxcr4a* mutant and misconnections, including MMCtA self-interconnections and CtA self-interconnections, increased (Fig. 2A,B,D-H). Because the *cxcr4a* mutant loses the majority of CtA to BA connections during development (Bussmann et al., 2011), to bypass the cerebrovascular developmental defects in the mutant, we took advantage of temporal administration of a Cxcr4 chemical inhibitor, AMD3100. Treatment with AMD3100 from 1 dpt to 4 dpt after injury led to loss of the peripheral-to-medial growing directionality of iLVs and nascent BVs (Fig. 2I-K) and the consequent failed formation of CtA to BA connections (Fig. 2I,J, asterisks). These results validate the requirement of Cxcr4a in the determination of iLV directionality. Loss of Cxcr4a makes iLVs lose the capability to sense the chemokine ligand. Thus, the iLVs cannot find the correct growth direction and generate misconnections in the mutant.

Although iLVs lost directionality in the *cxcr4a* mutant, time-lapse imaging at 3 dpt and 4 dpt showed that replenishment of Cxcr4a in the LECs after injury could re-direct the iLVs (Fig. 3A,B,D). When the *cxcr4a* mutant was placed under the *Tg(lyve1:CreER^{T2}; hsp70l:loxP-STOP-loxP-cxcr4a-p2A-Venus-cryaa-CFP; kdrl:DenNTR; lyve1b:DsRed)* transgenic background, in which the expression of Cxcr4a-p2A-Venus could be specifically induced in the LECs, the ingrowing direction of hindbrain iLVs could be re-directed from CtA to BA by the application of 4-hydroxytamoxifen (4-OHT) plus heat shock (Fig. 3A,B,D). By contrast, specific replenishment of Cxcr4a in the BECs was ineffective in countering the iLV misdirection in the *cxcr4a* mutant (Fig. 3C,D). As a consequence, although the *cxcr4a* mutant exhibited mal-developed brain BVs, including defective CtA-to-BA connections (Fig. S4A,B,D), these connections could be efficiently re-established after injury only if Cxcr4a was specifically replenished in the LECs, but not in the BECs (Fig. 3E-J). These data provide further evidence to demonstrate the pivotal role of the Cxcr4a-expressing LECs in determining the growing direction of iLVs and nascent BVs.

In the *cxcl12b* mutant, the iLVs and nascent BVs became highly branched and lost directionality at 3 dpt and 4 dpt (Fig. 2C-H). This phenotype might be caused by loss of the Cxcl12b ligand, so that the

Development (2022) 149, dev200729. doi:10.1242/dev.200729

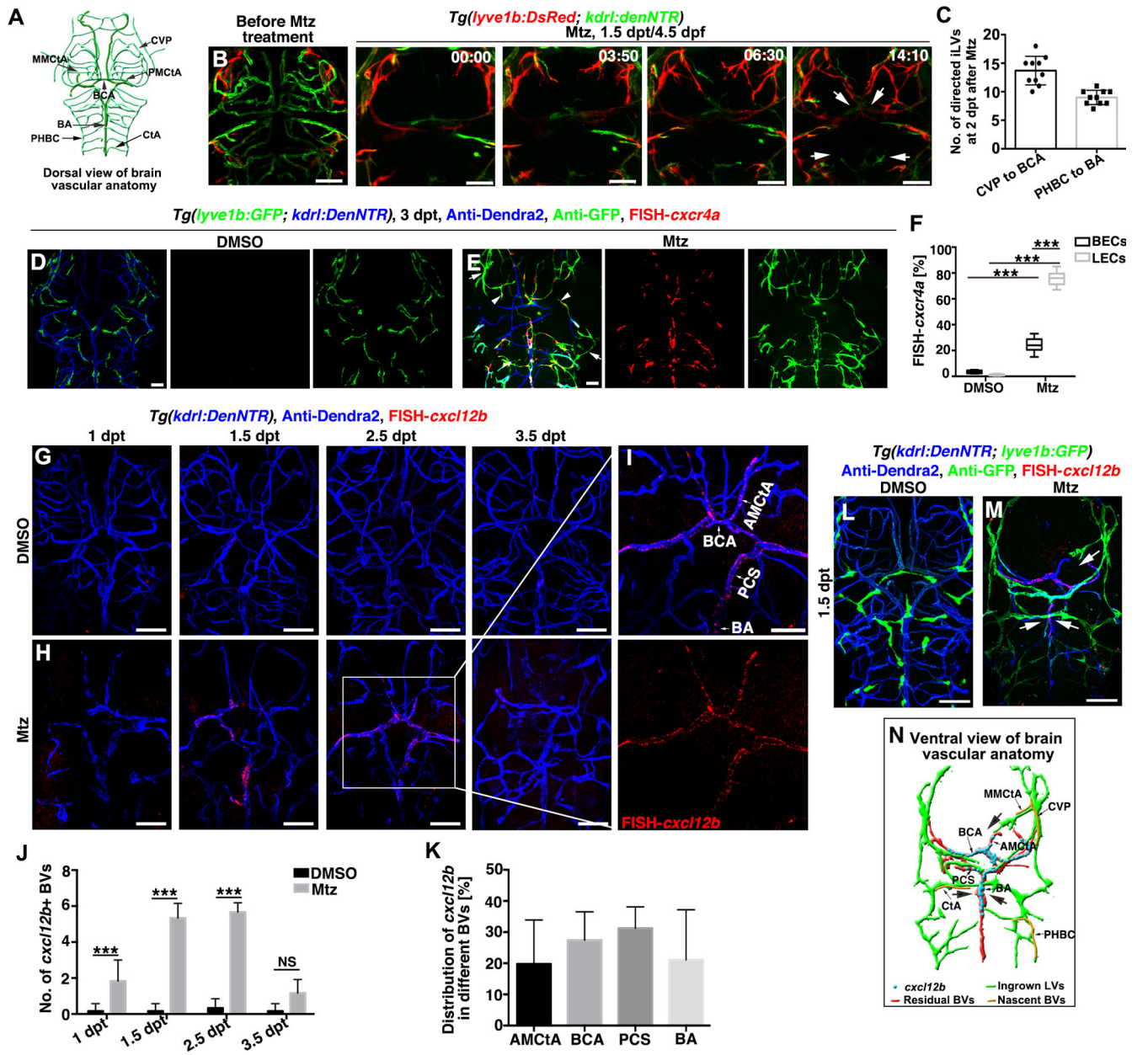

Fig. 1. *cxcr4a* and *cxcl12b* are transcriptionally activated in the iLVs and residual central BVs, respectively. (A) Schematic of zebrafish brain vascular anatomy at 4 dpf. (B) Brain vasculature at 3 dpf (before Mtz treatment) and the *lyve1b*+ ingrown lymphatic vessels (iLVs) ingrow from peripheral to the central injured parenchyma with clear directionality. Arrows indicate their directional ingrowth from choroidal vascular plexus (CVP) to basal communicating artery (BCA), and from primordial hindbrain channel (PHBC) to basilar artery (BA) (n=10/10), the elapsed time is indicated in h:min from 1.5 dpt/4.5 dpf. (C) Quantification of the number of directed iLVs at 2 dpt (n=10, mean±s.d.). (D-F) Triple labeling of FISH-*cxcr4a*, anti-GFP and Dendra2 at 3 dpt after DMSO (D, n=20/20) and Mtz (E, n=19/20) treatment. Arrowheads show that *cxcr4a* is localized in the central brain including the leading iLECs, arrows show that the peripheral LECs showed less or even no *cxcr4a*. Quantification shows the *cxcr4a* expression after DMSO and Mtz treatment (F, n=8, ***P<0.0001, two-way ANOVA by Sidak's multiple comparisons test). Box plot shows median values (middle bars) and first to third interquartile ranges (boxes) and whiskers represent the min-max range. (G-K) Double labeling of FISH-*cxcl12b* and anti-Dendra2 after DMSO (G, 1 dpt, n=16/16; 1.5 dpt, n=15/16; 2.5 dpt, n=21/22; 3.5 dpt, n=16/17) and Mtz (H, 1 dpt, n=26/32; 1.5 dpt, n=32/40; 2.5 dpt, n=40/42; 3.5 dpt, n=25/29) treatment. Magnified images show that *cxcl12b* is specifically expressed in the residual central blood vessels (BVs) including anterior mesencephalic central artery (AMCtA), BCA, posterior communicating segment (PCS) and BA (I). Statistics show the number of *cxcl12b*+ BVs (J, n=6, 1 dpt, ***P=0.0004; 1.5 dpt, ***P<0.0001; 2.5 dpt, ***P<0.0001; 3.5 dpt, NS=0.0548, two-way ANOVA by Sidak's multiple comparisons test, mean±s.d.) and the distribution of *cxcl12b* signals in different BVs (K, n=13, mean±s.d.). (L-N) In contrast to the uninjured control (L, n=15/16), the *lyve1b*+ iLVs ingrow towards the *cxcl12b*-expressing residual central BVs at 1.5 dpt after injury (M, n=18/20). Explanatory schematic of M is shown in N. Arrows indicate the ingrowing directions of iLVs. MMCtA, middle mesencephalic central artery; PMCtA, posterior (caudal) mesencephalic central artery. Dorsal view in A-C, ventral view in D-N. Scale bars: 50 µm.

Cxcr4a+ iLVs extended more branches to sense the ligand. Because Cxcr4a upregulation has been reported to increase the number of filopodia (Bussmann et al., 2011), the compensatory upregulation of *cxcr4a* in the *cxcl12b* mutant (Fig. S5A-E) could also contribute to the hyperbranched phenotype of the mutant. In addition, the proliferation of endothelial cells remained unaffected in the *cxcl12b* mutant (Fig. S5F-H). Again, the CtA-to-BA connections could not be efficiently re-established at 5 dpt after injury (Fig. S4A,C,D).

Development (2022) 149, dev200729. doi:10.1242/dev.200729

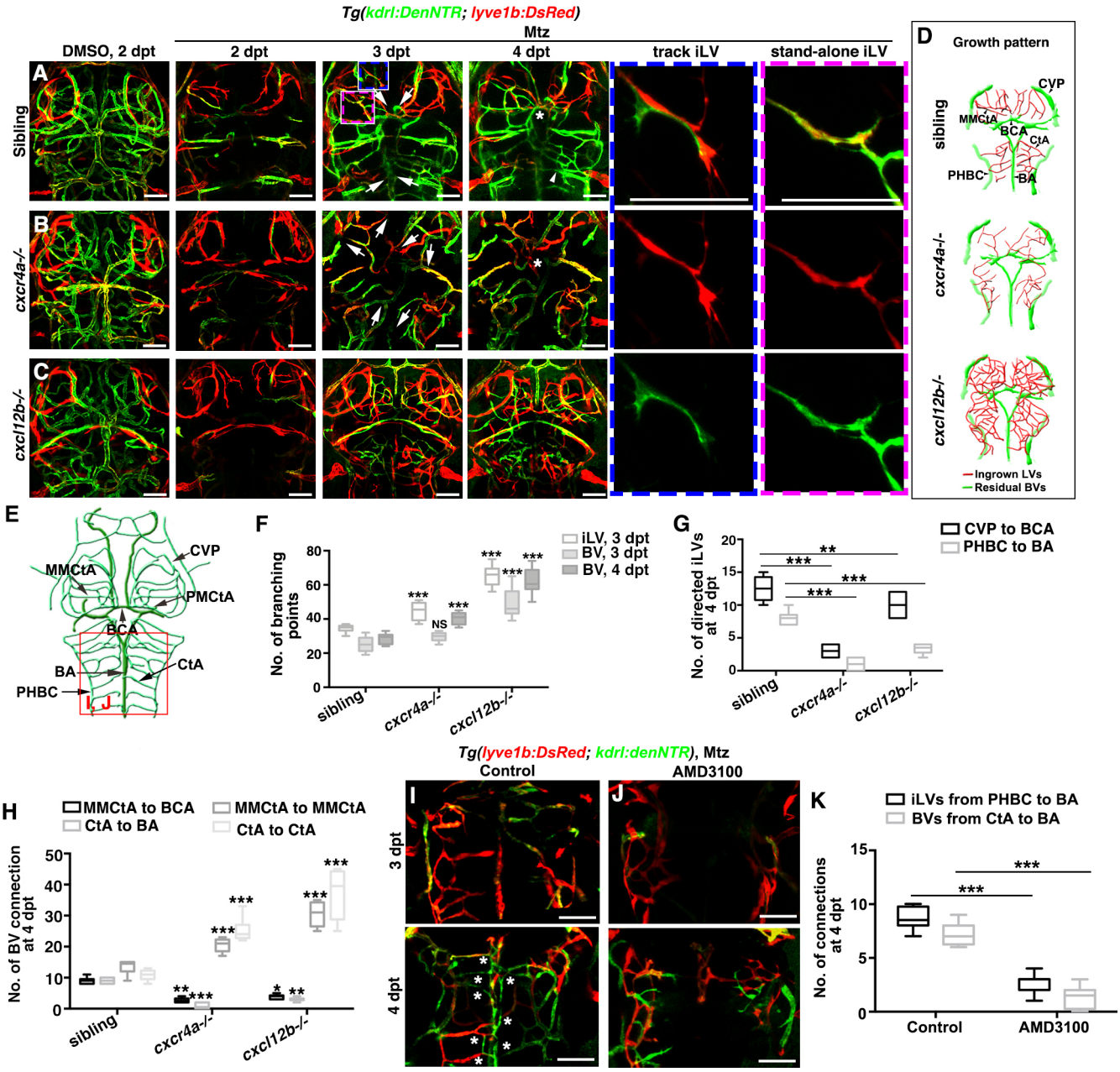

Fig. 2. Cxcl12b/Cxcr4a is required for determining the ingrowing direction of iLVs and nascent BVs. (A-H) In the *cxcr4a* mutant, the ingrown lymphatic vessels (iLVs) and blood vessels (BVs) lose their peri-to-medial directions (B, arrows, *n*=19/19) as indicated in the sibling (A, arrows, *n*=32/33). Asterisks indicate the connection of middle mesencephalic central artery (MMCtA) to basal communicating artery (BCA) (A,B). Both track iLVs (blue dashed box enlarged in A) and standalone iLVs (purple dashed box enlarged in A) in siblings migrate with directionality. In the *cxcl12b* mutant, iLVs and nascent BVs become hyperbranched and randomized (C, *n*=21/25). Explanatory schematics illustrate the vessel growth pattern (D). Schematic of brain vascular anatomy and red box indicates the image areas in the corresponding panels (E). Quantification shows the number of vessel branching points [F, *n*=8, sibling versus *cxcr4a*−/−, iLV, 3 dpt, ***P=0.0007; BV, 3 dpt, not significant (NS), P=0.1624; BV, 4 dpt, ***P<0.0001; sibling versus *cxcl12b*−/−, ***P<0.0001], the number of directed iLVs at 4 dpt (G, *n*=6, ***P<0.0001, **P=0.0055), and the number of BV connections at 4 dpt (H, *n*=6, sibling versus *cxcr4a*−/−, **P=0.0019, ***P<0.0001; sibling versus *cxcl12b*−/−, *P=0.0123, **P=0.0033, ***P<0.0001). (I-K) Compared with the control (I, *n*=15/16, asterisks), after AMD3100 treatment the iLVs and BVs lost peri-to-medial directions (J, *n*=20/22). Quantification shows the number of directed iLVs [from primordial hindbrain channel (PHBC) to basilar artery (BA)] and BV connections from central artery (CtA) to BA (K, *n*=8, ***P<0.0001). Two-way ANOVA by Sidak's multiple comparisons test. Box plots show median values (middle bars) and first to third interquartile ranges (boxes) and whiskers represent the min-max range. CVP, choroidal vascular plexus; LV, lymphatic vessel; PMCtA, posterior (caudal) mesencephalic central artery. Dorsal view. Scale bars: 50 µm.

Although the iLVs and nascent BVs lost proper direction in both *cxcr4a* and *cxcl12b* mutants, nascent BVs kept growing along iLVs, and the standalone iLVs kept transdifferentiating (Fig. S6). These data indicate that although Cxcl12b/Cxcr4a is required for determining the directionality of iLVs and in turn nascent BVs, it is dispensable for the iLV transdifferentiation or vessel growth.

To investigate whether Cxcl12b/Cxcr4a-mediated chemotaxis is sufficient to direct the iLV ingrowth, an *hsp70l:venus-p2A-cxcl12b* plasmid driven by the heat shock promoter was administered for ectopic, mosaic expressions of Cxcl12b in the *cxcl12b* mutant (Fig. 4A). The ectopically expressed Cxcl12b, but not the control Venus protein, attracted

Development (2022) 149, dev200729. doi:10.1242/dev.200729

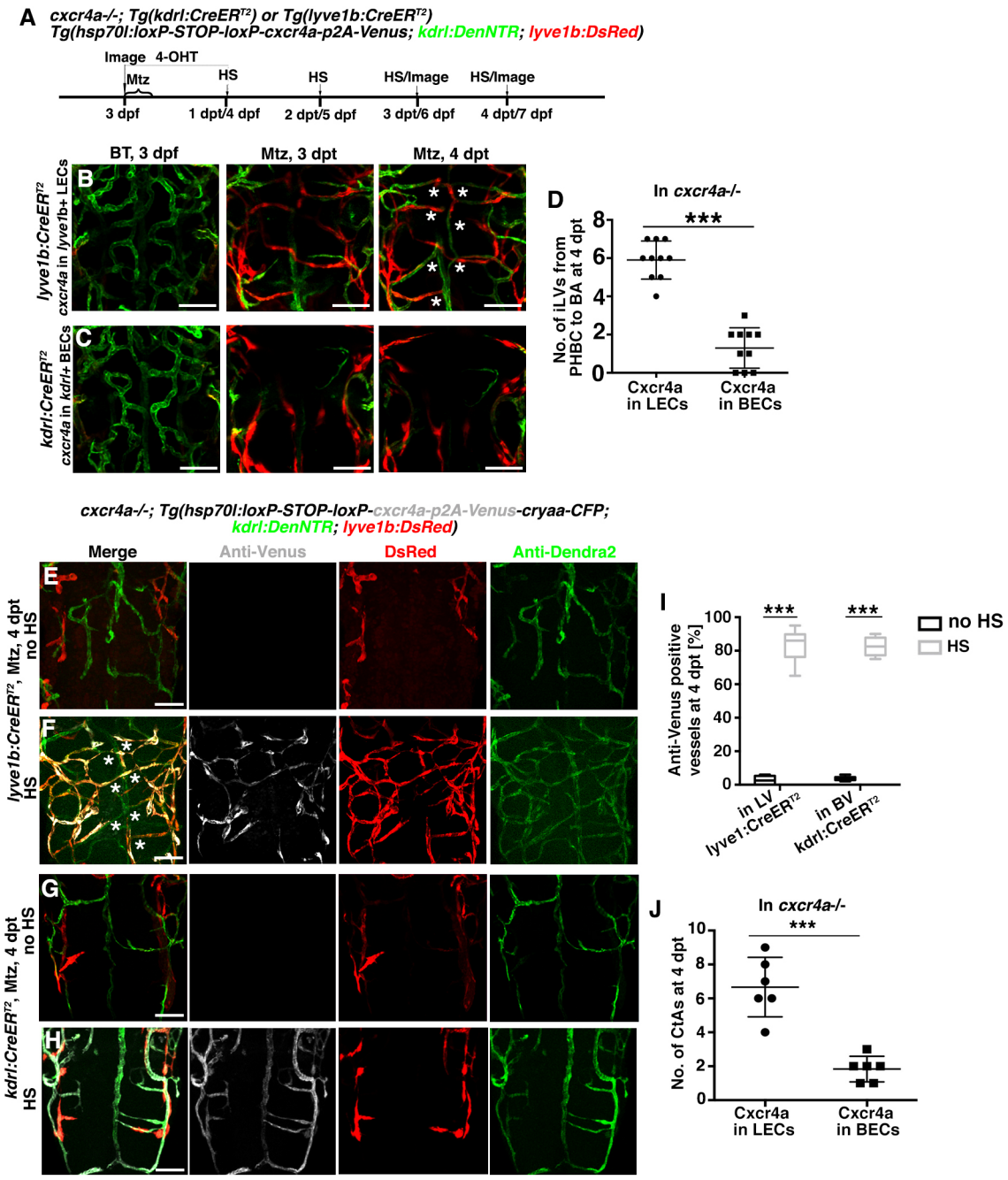

Fig. 3. Cxcr4a in LECs is required for the iLV directionality during BV regeneration. (A-D) The transgenic lines and time points of Mtz, 4-OHT and heat shock (HS) administrations are shown in A. In *cxcr4a* mutants, time-lapse imaging at 3 dpt and 4 dpt showed that replenishment of Cxcr4a in the lymphatic endothelial cells (LECs) (B, n=11/16) but not in the blood endothelial cells (BECs) (C, n=8/12) after injury could re-direct the ingrown lymphatic vessels (iLVs). Asterisks indicate connections of central artery (CtA) to basilar artery (BA). Quantification shows the number of directed iLVs from primordial hindbrain channel (PHBC) to BA at 4 dpt (D, n=10, ***P<0.0001, two-tailed unpaired t-test, mean±s.d.). (E-J) Controlled by the no HS (E, n=15/15; G, n=13/14), the CtA to BA connections were efficiently re-established after injury only if Cxcr4a was specifically replenished in the LECs (F, n=18/23), but not in the BECs (H, n=17/19). Asterisks indicate connections of CtA to BA. Quantification shows the ratio of anti-Venus+ vessels at 4 dpt (I, n=6, ***P<0.0001, two-way ANOVA by Sidak's multiple comparisons test) and the number of CtAs in F and H (J, n=6, ***P<0.0001, two-tailed unpaired t-test, mean±s.d.). Box plot shows median values (middle bars) and first to third interquartile ranges (boxes) and whiskers represent the min-max range. Dorsal view in B and C. Ventral view in E-H. Scale bars: 50 µm.

iLV sprouts towards the ectopic sites (Fig. 4B-D; Movie 3). These data indicate that Cxcl12b/Cxcr4a is not only necessary, but also sufficient, for determining the directionality of iLV ingrowth.

In summary, after brain vascular injury, *cxcr4a* and *cxcl12b* are transcriptionally activated in the iLVs and residual central BVs, respectively, which are required and sufficient for determining the growing directionality of iLVs and in turn nascent BVs (Fig. 4E).

Chemokine signaling is required for cerebrovascular patterning during development (Bussmann et al., 2011; Fujita et al., 2011). This is consistent with our results that Cxcl12b/Cxcr4a signaling controls the vessel patterning during cerebrovascular regeneration. However, different from the direct regulation of Cxcr4a on brain angiogenesis during development, here, the function of Cxcr4a in the guidance of neoangiogenesis is an indirect rather than a direct effect,

Development (2022) 149, dev200729. doi:10.1242/dev.200729

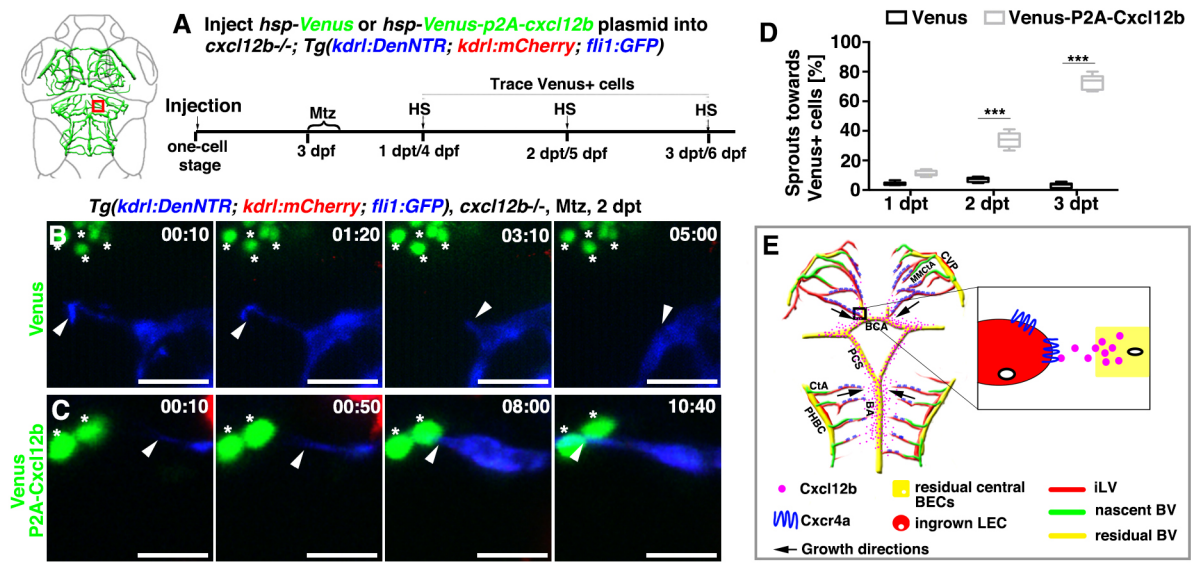

Fig. 4. Cxcl12b/Cxcr4a is sufficient to direct iLV ingrowth and cerebrovascular regeneration. (A) Illustrations of the method, transgenic lines and time points of heat shock (HS). Red box indicates the image area. (B-D) In the *cxcl12b* mutant, ectopically expressed Venus-p2A-Cxcl12b (C, asterisks, *n*=12/14), but not Venus (B, asterisks, *n*=15/15), is sufficient to attract ingrown lymphatic vessels (iLV) sprouts (arrowheads). Dorsal view. The elapsed time is indicated in h:min from 2 dpt. Quantification shows ratios of the sprouts growing toward the ectopic sites (D, *n*=8 larvae, every larva was traced about 20 Venus+ cells, ***P<0.0001, two-way ANOVA by Sidak's multiple comparisons test). Box plot shows median values (middle bars) and first to third interquartile ranges (boxes) and whiskers represent the min-max range. Scale bars: 20 µm. (E) Schematic of Cxcl12b-Cxcr4a signaling directing iLV ingrowth and cerebrovascular regeneration. BCA, basal communicating artery; BV, blood vessel; CtA, central artery; CVP, choroidal vascular plexus; LEC, lymphatic endothelial cell; MMCtA, middle mesencephalic central artery; PHBC, primordial hindbrain channel.

which is mediated by determining the directionality of iLVs. Cxcr4a determines the growing directionality of nascent BVs (through iLVs), but it is not required for the vessel growth itself (Fig. S6). Our previous work has reported that the iLECs produce Vegfa to promote blood vessel growth (Chen et al., 2019). Furthermore, previous studies have reported that the regulations of HUVEC cell migration and PHBC sprouting by Cxcl12/Cxcr4 are mediated by the PI3K-Akt-eNOS signaling pathway (Fujita et al., 2011; Zheng et al., 2007). Whether the Cxcl12b/Cxcr4a-directed iLV ingrowth is also mediated via PI3K signaling requires further investigation.

Besides cerebrovascular regeneration, collateralization in response to cerebral hypoxia is another important neoangiogenesis process in the brain (Liu et al., 2014). The establishment of collateral vessels normally occurs before complete occlusion of brain BVs, which prevents patients from suffering ischemic stroke. Cxcr4 is also positively correlated with the presence and extent of angiographic coronary collaterals in patients with coronary occlusion (Yang et al., 2016). In zebrafish, collateral vessel formation depends on Cxcr4 signaling (Packham et al., 2009). It is possible that cerebrovascular regeneration and collateralization apply similar cellular and molecular mechanisms. Thus, promotion of directional lymphangiogenesis by combination of pro-lymphangiogenic drugs and CXCL12/CXCR4-related drugs provides potential strategies for developing translatable post-ischemic and/or pre-ischemic therapies.

MATERIALS AND METHODS

Zebrafish strains

The zebrafish facility and study were approved by the Institutional Review Board of Southwest University (Chongqing, China). Zebrafish were maintained in accordance with the Guidelines of Experimental Animal Welfare from the Ministry of Science and Technology of China (2006) and the Institutional Animal Care and Use Committee protocols from Southwest University (2007). Embryos were treated with 0.003% 1-phenyl-2-thiourea (PTU, Sigma-Aldrich) to inhibit pigment formation. The *Tg(kdrl:Dendra2-NTR)*^{cq10} (Chen et al., 2019), *Tg(kdrl:mCherry)*^{cq15} (Chen et al., 2019), *Tg(fli1:GFP)*^{y1} (Lawson and Weinstein, 2002), *Tg(prox1a*^{BAC}*:KalTA4; UAS:TagRFP)*^{nim5} (van Impel et al., 2014), *Tg(lyve1b:DsRed)*^{cq27} (Chen et al., 2019), *Tg(lyve1b:CreER*^{T2}*)*^{cq25} (Chen et al., 2019), *Tg(kdrl:CreER*^{T2}*)*^{cq24} (Zhan et al., 2018), *Tg(abcc9*^{BAC}*:Gal4FF)*^{ncv34} (Ando et al., 2019), *cxcr4a*^{um20} mutant (Bussmann et al., 2011) and *cxcl12b*^{mu100} mutant (Bussmann et al., 2011) were used in this study.

Generation of transgenic zebrafish

For constructing the *hsp70l:Loxp-STOP-Loxp-cxcr4a- p2A-Venus* plasmid, we first amplified the full-length zebrafish *cxcr4a* cDNA using the primers 5′-ATGGCTTATTACGAACACATCG-3′ and 5′-ACTAGAGT-GAAAGCTGGAAGAT-3′, then overlapped the *cxcr4a* sequence with the *p2A-Venus* sequence using overlap PCR. *hsp70l:loxP-mCherry-STOP-loxP-H2B-GFP-cryaa-cerulean* (Addgene plasmid #24334) plasmid was digested by XhoI to remove the *mCherry* fragment, followed by replacement of the *H2B-GFP* cassette with *cxcr4a-p2A-Venus* to construct the *hsp70l:loxP-STOP-loxP-cxcr4a-p2A-Venus-cryaa-cerulean* plasmid. *Tg(hsp70l:loxp-STOP-loxp-cxcr4a-p2A-Venus)*^{cq26} transgenic line was generated using the pBluescript vector. Constructs flanked by the I-SceI restriction sites were co-injected with I-SceI (New England Biolabs) into zebrafish embryos of the AB genetic background at the one-cell stage for transgenesis. The embryos were screened for the lenses that expressed the cyan fluorescent protein (CFP), then raised to adulthood and crossed to identify founder fish with germline integration.

cxcr4a^{BAC}*-TagRFP* (70-80 pg) was co-injected with the capped *tol2 transposase* RNA (40-50 pg) for transgenesis [*Tg(cxcr4aBAC:TagRFP)*^{cq14}]. After injection, embryos were screened for fin-expressed red fluorescent protein under microscope and then bred to adulthood and outcrossed with AB genetic background to get the germline transmissions.

Live imaging

For time-lapse live imaging, zebrafish embryos were grown in the presence of 0.003% PTU to avoid pigmentation. Larvae were mounted in 1.2% low melting point agarose in the egg water with 0.003% PTU using 35 mm glass-bottom dishes (Liu et al., 2016; Yang et al., 2021). Time-lapse images were captured using a 20× water immersion objective mounted on the Zeiss LSM780NLO confocal microscope equipped with a heating stage to

Development (2022) 149, dev200729. doi:10.1242/dev.200729

maintain 28.5°C. *Z*-stack images were collected every 5-10 min, and three-dimensional datasets were compiled using ZEN2010 software (Carl Zeiss).

Antibody staining

Zebrafish whole-mount antibody staining was performed as previously described (Lu et al., 2013; Chen et al., 2019; Cao et al., 2019). Primary antibodies used in the study were: GFP (1:500; Abcam, ab6658; Santa Cruz Biotechnology, sc9996), Dendra2 (1:500; Antibodies-online, ABIN361314), Prox1 (1:1000; Abcam, ab5475), TagRFP or RFP (1:500; Abnova, MAB9754), Venus (1:500; Santa Cruz Biotechnology, sc9996), DsRed (1:500; Santa Cruz Biotechnology, sc101526). Secondary antibodies used in the study were: donkey anti-goat IgG Alexa Fluor 488-conjugated (1:1000; Invitrogen, A11055), donkey anti-goat IgG Alexa Fluor 633-conjugated (1:1000; Invitrogen, A21082), donkey anti-goat IgG Alexa Fluor 405-conjugated (1:1000; Abcam, ab175664), donkey anti-mouse IgG Alexa Fluor 568-conjugated (1:1000; Invitrogen, A10037), donkey anti-mouse IgG Alexa Fluor 647-conjugated (1:1000; Invitrogen, A31571), donkey anti-rabbit IgG Alexa Fluor 647-conjugated (1:1000; Invitrogen A31573), donkey anti-rabbit IgG Alexa Fluor 488-conjugated (1:1000; Invitrogen, A21206), goat anti-rabbit IgG Alexa Fluor 405-conjugated (1:1000; Invitrogen, A31556). Antibody stained or live larvae were mounted in 1.2% low melting point agarose and imaged using ZEN2010 software equipped on an LSM780 confocal microscope (Carl Zeiss).

Combination of FISH and antibody staining

The combination of fluorescence *in situ* hybridization (FISH) and antibody staining was performed as previously described (He et al., 2014, 2019, 2020) using *cxcr4a*, *cxcl12b* and *vegfr3* digoxigenin-labeled probes. The *cxcr4a*, *cxcl12b* and *vegfr3* (Chen et al., 2019) probes synthesized from PCR templates are able to avoid the off-target hybridization to tissues expressing transgenes (Cha and Weinstein, 2012). In our method, the PCR-amplified sequence of a gene of interest is used as a template for the synthesis of an antisense RNA probe, which is labeled with digoxigenin or fluorescein-linked nucleotides. Afterwards, antibody staining proceeded as described above. The *Tg(kdrl:DenNTR; fli1:GFP)* or *Tg(lyve1b:GFP; kdrl:DenNTR)* lines were subjected to antibody staining using the anti-GFP (1:1000; Santa Cruz Biotechnology, sc9996) and anti-Dendra2 (1:1000; Antibodies-online, ABIN361314) primary antibodies. Then, the goat anti-mouse IgG Alexa Fluor 633-conjugated (1:1000; Invitrogen, A21052) and goat anti-rabbit IgG Alexa Fluor 405-conjugated (1:1000; Invitrogen, A31556) secondary antibodies were used to label GFP and Dendra2, respectively. The *Tg(prox1:TagRFP; kdrl:DenNTR)* or *Tg(kdrl:DenNTR; cxcr4a*^{BAC}*:TagRFP)* lines were subjected to antibody staining using the anti-TagRFP (1:500; Abnova, MAB9754) and anti-Dendra2 (1:1000; Antibodies-online, ABIN361314) primary antibodies. Then, the donkey anti-mouse IgG Alexa Fluor 568-conjugated (1:1000; Invitrogen, A10037) and goat anti-rabbit IgG Alexa Fluor 405-conjugated (1:1000; Invitrogen, A31556) secondary antibodies were used to label RFP and Dendra2, respectively.

Cell sorting and quantitative real-time PCR

For cell sorting, 150 brains of the *Tg(kdrl:DenNTR; lyve1b:DsRed)* larvae were dissected, and the DsRed+ cells (~13,000 cells) from uninjured larvae at 6 dpf (days postfertilization) and the DsRed+ cells (~16,420 cells) from regenerated larvae at 3 dpt/6 dpf, were sorted by fluorescence-activated cell sorting (FACS) as previously described (Chen et al., 2019). The total RNA was extracted by TRIzol reagent (Roche). cDNA was synthesized using the Reverse Transcription Kit (Roche).

Quantitative real-time PCRs (qPCRs) were carried out using the following primers (5′ to 3′) for *cxcr4a*: CATGACAGACAAGTACCGTCT and TGCTGTACAAGTTTACCGTGTA (Peng et al., 2022). qPCR using the FastStart Universal SYBR Green Master (Roche) was normalized by transcriptions of *eef1a1l1*: 5′-TTCTGTTACCTGGCAAAGGG-3′ and 5′-TTCAGTTTGTCCAACACCCA-3′.

Temporal control of CreER^{T2} activities and heat shock

4-OHT (Sigma-Aldrich) was dissolved in 100% ethanol to prepare a stock concentration of 10 mmol/l. Larvae were incubated in 5 µM working solution at the indicated time frame using 0.05% ethanol in egg water as control. For the BEC or LEC specific overexpression Cxcr4a-P2A-Venus, the *cxcr4a−/−*; *Tg(kdrl:CreER*^{T2}*; hsp70l:loxP-STOP-loxsP-cxcr4a-p2A-Venus; cryaa-CFP; kdrl:DenNTR; lyve1b:DsRed)* and *cxcr4a−/−*; *Tg(lyve1b:CreER*^{T2}*; hsp70l:loxP-STOP-loxP-cxcr4a-p2A-Venus; cryaa-CFP; kdrl:DenNTR; lyve1b:DsRed)* larvae were first screened for the lens-expressing CFP. During incubation with 4-OHT from 3 dpf to 1 dpt/4 dpf, heat shock was carried out at 38.5°C for 40 min. Then, heat shock was repeatedly performed every 24 h from 1 dpt to 4 dpt. Afterwards, these larvae were subjected to time-lapse imaging and antibody staining.

Chemical treatment

Mtz treatment was performed as previously described (Chen et al., 2019). Larvae at 3 dpf were incubated with 1 mM Mtz (Sigma-Aldrich) in 0.2% DMSO for 5 h, washed three times with egg water, and recovered in the egg water with 0.003% PTU. We defined 19 h after withdrawal of Mtz as 1 dpt, which is equivalent to 4 dpf.

AMD3100 (AdooQ, 110078-46-1) treatment was performed as previously described (Peng et al., 2022). Larvae were treated with 20 µM Cxcr4 antagonist AMD3100 diluted in fish water from 1 dpt to 4 dpt.

Mosaic ectopic expressions

For ectopic expression of Cxcl12b, the *Venus-p2A-cxcl12b* and *Venus* cassettes were inserted between the SalI and NotI sites in the *hsp70l:cryaa-cerulean* vector to construct the *hsp70l:Venus-p2A-cxcl12b-cryaa-cerulean* and *hsp70l:Venus-cryaa-cerulean* plasmids, respectively. Plasmids were injected at the one-cell stage into the blastomeres of *cxcl12b* mutant embryos under a *Tg(kdrl:DenNTR; kdrl:mCherry; fli1:GFP)* transgenic background. Then, heat shock (38.5°C for 40 min) was repeatedly performed every 24 h from 1 dpt to 3 dpt. After heat shock, the larvae were first screened for Venus expression in the brain under microscope, then the larvae were mounted in 1.2% low melting point agarose for time-lapse live imaging. Venus+ cells were traced and imaged using ZEN2010 software equipped on an LSM780 confocal microscope (Carl Zeiss).

Edu labeling

EdU labeling was performed as previously described (Cai et al., 2021). We injected the EdU (500 µM) into the heart of larvae at 1 dpt and fixed the sample after 2 days post injection followed by using the Click-iT EdU Kit (Invitrogen) to label the proliferating cells according to the manufacturer's instructions.

Quantification and statistical analysis

All statistical calculations were performed using GraphPad Prism. Variance of data for all groups is presented as mean±s.d. (bar charts) or the min-max range (box plots). Box plots show median values (middle bars) and first to third interquartile ranges (boxes). All experiments were performed with larval zebrafish. Larvae were collected from incrosses and outcrosses of several pairs of adult zebrafish. Mutant and sibling larvae were grown together in a single tank. Phenotyping preceded genotyping in mutant analyses, hence analysis was genotype blinded. In the other experiments, the investigators were not blinded to group allocation during data collection and/or analysis. All experiments comparing treatment groups were carried out using randomly assigned siblings. After at least two repeated experiments, data were analyzed for statistical significance using two-way ANOVA by Sidak's multiple comparisons test, and two-tailed unpaired *t*-test. A value of $P<0.05$ was considered to be statistically significant. No data were excluded from analyses. The exact sample size (n), P-value for each experimental group and statistical tests are indicated in the figure legends.

Acknowledgements

We thank Arndt F. Siekmann (Max Planck Institute for Molecular Biomedicine, Münster, Germany) for the mutant lines (*cxcr4a* mutant and *cxcl12b* mutant), Brant M. Weinstein (National Institutes of Health, Bethesda, MD, USA) for the *cxcr4a*^{BAC}*:TagRFP* plasmid, Koji Ando (Uppsala University, Sweden) for the *abcc9*^{BAC}*:Gal4* transgenic line, Philip S. Crosier (University of Auckland, New Zealand) for the *lyve1b* plasmids, Li Li (Southwest University, China) and Nathan D. Lawson (University of Massachusetts, Worcester) for discussions.

Competing interests
The authors declare no competing or financial interests.

Author contributions
Conceptualization: J.H.; Methodology: J.C., J.H.; Validation: J.H.; Formal analysis: J.C.; Investigation: J.C., J.H.; Data curation: J.C.; Writing - original draft: J.C., L.L.; Writing - review & editing: L.L.; Visualization: J.C.; Supervision: L.L.; Project administration: L.L.; Funding acquisition: J.C., L.L.

Funding
This work was supported by the National Key Research and Development Program of China (2021YFA0805000), the National Natural Science Foundation of China (32192400, 32000576, 31730060), and the Natural Science Foundation of Chongqing (cstc2020jcyj-msxmX0882).

Peer review history
The peer review history is available online at https://journals.biologists.com/dev/article-lookup/doi/10.1242/dev.200729.

References

Ando, K., Wang, W., Peng, D., Chiba, A., Lagendijk, A. K., Barske, L., Crump, J. G., Stainier, D. Y. R., Lendahl, U., Koltowska, K. et al. (2019). Peri-arterial specification of vascular mural cells from naïve mesenchyme requires Notch signaling. *Development* **146**, dev165589. doi:10.1242/dev.165589

Aspelund, A., Antila, S., Proulx, S. T., Karlsen, T. V., Karaman, S., Detmar, M., Wiig, H. and Alitalo, K. (2015). A dural lymphatic vascular system that drains brain interstitial fluid and macromolecules. *J. Exp. Med.* **212**, 991-999. doi:10.1084/jem.20142290

Bower, N. I., Koltowska, K., Pichol-Thievend, C., Virshup, I., Paterson, S., Lagendijk, A. K., Wang, W., Lindsey, B. W., Bent, S. J., Baek, S. et al. (2017). Mural lymphatic endothelial cells regulate meningeal angiogenesis in the zebrafish. *Nat. Neurosci.* **20**, 774-783. doi:10.1038/nn.4558

Bussmann, J., Bos, F. L., Urasaki, A., Kawakami, K., Duckers, H. J. and Schulte-Merker, S. (2010). Arteries provide essential guidance cues for lymphatic endothelial cells in the zebrafish trunk. *Development* **137**, 2653-2657. doi:10.1242/dev.048207

Bussmann, J., Wolfe, S. A. and Siekmann, A. F. (2011). Arterial-venous network formation during brain vascularization involves hemodynamic regulation of chemokine signaling. *Development* **138**, 1717-1726. doi:10.1242/dev.059881

Cai, P., Mao, X., Zhao, J., Nie, L., Jiang, Y., Yang, Q., Ni, R., He, J. and Luo, L. (2021). Farnesoid X receptor is required for the redifferentiation of bipotential progenitor cells during biliary-mediated zebrafish liver regeneration. *Hepatology* **74**, 3345-3361. doi:10.1002/hep.32076

Cao, Z., Mao, X. and Luo, L. (2019). Germline stem cells drive ovary regeneration in Zebrafish. *Cell Rep* **26**, 1709-1717. doi:10.1016/j.celrep.2019.01.061

Castranova, D., Samasa, B., Venero Galanternik, M., Jung, H. M., Pham, V. N. and Weinstein, B. M. (2021). Live imaging of intracranial lymphatics in the Zebrafish. *Circ. Res.* **128**, 42-58. doi:10.1161/CIRCRESAHA.120.317372

Cha, Y. R. and Weinstein, B. M. (2012). Use of PCR template-derived probes prevents off-target whole mount in situ hybridization in transgenic zebrafish. *Zebrafish* **9**, 85-89. doi:10.1089/zeb.2011.0731

Cha, Y. R., Fujita, M., Butler, M., Isogai, S., Kochhan, E., Siekmann, A. F. and Weinstein, B. M. (2012). Chemokine signaling directs trunk lymphatic network formation along the preexisting blood vasculature. *Dev. Cell* **22**, 824-836. doi:10.1016/j.devcel.2012.01.011

Chen, J., He, J., Ni, R., Yang, Q., Zhang, Y. and Luo, L. (2019). Cerebrovascular injuries induce lymphatic invasion into brain parenchyma to guide vascular regeneration in Zebrafish. *Dev. Cell* **49**, 697-710. doi:10.1016/j.devcel.2019.03.022

Chen, J., Li, X., Ni, R., Chen, Q., Yang, Q., He, J. and Luo, L. (2021). Acute brain vascular regeneration occurs via lymphatic transdifferentiation. *Dev. Cell.* **56**, 3115-3127. doi:10.1016/j.devcel.2021.09.005

Fujita, M., Cha, Y. R., Pham, V. N., Sakurai, A., Roman, B. L., Gutkind, J. S. and Weinstein, B. M. (2011). Assembly and patterning of the vascular network of the vertebrate hindbrain. *Development* **138**, 1705-1715. doi:10.1242/dev.058776

Gancz, D., Raftrey, B. C., Perlmoter, G., Marín-Juez, R., Semo, J., Matsuoka, R. L., Karra, R., Raviv, H., Moshe, N., Addadi, Y. et al. (2019). Distinct origins and molecular mechanisms contribute to lymphatic formation during cardiac growth and regeneration. *Elife* **8**, e44153. doi:10.7554/eLife.44153

Grunewald, M., Avraham, I., Dor, Y., Bachar-Lustig, E., Itin, A., Jung, S., Chimenti, S., Landsman, L., Abramovitch, R. and Keshet, E. (2006). VEGF-induced adult neovascularization: recruitment, retention, and role of accessory cells. *Cell* **124**, 175-189. doi:10.1016/j.cell.2005.10.036

Harrison, M. R., Bussmann, J., Huang, Y., Zhao, L., Osorio, A., Burns, C. G., Burns, C. E., Sucov, H. M., Siekmann, A. F. and Lien, C. L. (2015). Chemokine-guided angiogenesis directs coronary vasculature formation in zebrafish. *Dev. Cell* **33**, 442-454. doi:10.1016/j.devcel.2015.04.001

Harrison, M. R., Feng, X., Mo, G., Aguayo, A., Villafuerte, J., Yoshida, T., Pearson, C. A., Schulte-Merker, S. and Lien, C. L. (2019). Late developing cardiac lymphatic vasculature supports adult zebrafish heart function and regeneration. *Elife* **8**, e42762. doi:10.7554/eLife.42762

He, J., Chen, J., Wei, X., Leng, H., Mu, H., Cai, P. and Luo, L. (2019). Mammalian target of rapamycin complex 1 signaling is required for the dedifferentiation from biliary cell to Bipotential progenitor cell in Zebrafish liver regeneration. *Hepatology* **70**, 2092-2106. doi:10.1002/hep.30790

He, J., Lu, H., Zou, Q. and Luo, L. (2014). Regeneration of liver after extreme hepatocyte loss occurs mainly via biliary transdifferentiation in zebrafish. *Gastroenterology* **146**, 789-800. doi:10.1053/j.gastro.2013.11.045

He, J., Mo, D., Chen, J. and Luo, L. (2020). Combined whole-mount fluorescence in situ hybridization and antibody staining in zebrafish embryos and larvae. *Nat. Protoc.* **15**, 3361-3379. doi:10.1038/s41596-020-0376-7

Isogai, S., Horiguchi, M. and Weinstein, B. M. (2001). The vascular anatomy of the developing zebrafish: an atlas of embryonic and early larval development. *Dev. Biol.* **230**, 278-301. doi:10.1006/dbio.2000.9995

Jin, D. K., Shido, K., Kopp, H. G., Petit, I., Shmelkov, S. V., Young, L. M., Hooper, A. T., Amano, H., Avecilla, S. T., Heissig, B. et al. (2006). Cytokine-mediated deployment of SDF-1 induces revascularization through recruitment of CXCR4+ hemangiocytes. *Nat. Med.* **12**, 557-567. doi:10.1038/nm1400

Küchler, A. M., Gjini, E., Peterson-Maduro, J., Cancilla, B., Wolburg, H. and Schulte-Merker, S. (2006). Development of the zebrafish lymphatic system requires VEGFC signaling. *Curr. Biol.* **16**, 1244-1248. doi:10.1016/j.cub.2006.05.026

Lawson, N. D. and Weinstein, B. M. (2002). In vivo imaging of embryonic vascular development using transgenic zebrafish. *Dev. Biol.* **248**, 307-318. doi:10.1006/dbio.2002.0711

Li, W., Kohara, H., Uchida, Y., James, J. M., Soneji, K., Cronshaw, D. G., Zou, Y. R., Nagasawa, T. and Mukouyama, Y. S. (2013). Peripheral nerve-derived CXCL12 and VEGF-A regulate the patterning of arterial vessel branching in developing limb skin. *Dev. Cell* **24**, 359-371. doi:10.1016/j.devcel.2013.01.009

Liu, J., Wang, Y., Akamatsu, Y., Lee, C. C., Stetler, R. A., Lawton, M. T. and Yang, G. Y. (2014). Vascular remodeling after ischemic stroke: mechanisms and therapeutic potentials. *Prog. Neurobiol.* **115**, 138-156. doi:10.1016/j.pneurobio.2013.11.004

Liu, C., Wu, C., Yang, Q., Gao, J., Li, L., Yang, D. and Luo, L. (2016). Macrophages mediate the repair of brain vascular rupture through direct physical adhesion and mechanical traction. *Immunity* **44**, 1162-1176. doi:10.1016/j.immuni.2016.03.008

Louveau, A., Smirnov, I., Keyes, T. J., Eccles, J. D., Rouhani, S. J., Peske, J. D., Derecki, N. C., Castle, D., Mandell, J. W., Lee, K. S. et al. (2015). Structural and functional features of central nervous system lymphatic vessels. *Nature* **523**, 337-341. doi:10.1038/nature14432

Lu, H., Ma, J., Yang, Y., Shi, W. and Luo, L. (2013). EpCAM is an endoderm-specific Wnt derepressor that licenses hepatic development. *Dev. Cell* **24**, 543-553. doi:10.1016/j.devcel.2013.01.021

Navaratna, D., Guo, S., Arai, K. and Lo, E. H. (2009). Mechanisms and targets for angiogenic therapy after stroke. *Cell Adh. Migr.* **3**, 216-223. doi:10.4161/cam.3.2.8396

Okuda, K. S., Astin, J. W., Misa, J. P., Flores, M. V., Crosier, K. E. and Crosier, P. S. (2012). lyve1 expression reveals novel lymphatic vessels and new mechanisms for lymphatic vessel development in zebrafish. *Development* **139**, 2381-2391. doi:10.1242/dev.077701

Packham, I. M., Gray, C., Heath, P. R., Hellewell, P. G., Ingham, P. W., Crossman, D. C., Milo, M. and Chico, T. J. (2009). Microarray profiling reveals CXCR4a is downregulated by blood flow in vivo and mediates collateral formation in zebrafish embryos. *Physiol. Genomics* **38**, 319-327. doi:10.1152/physiolgenomics.00049.2009

Peng, D., Ando, K., Hußmann, M., Gloger, M., Skoczylas, R., Mochizuki, N., Betsholtz, C., Fukuhara, S., Schulte-Merker, S., Lawson, N. D. et al. (2022). Proper migration of lymphatic endothelial cells requires survival and guidance cues from arterial mural cells. *Elife* **11**, e74094. doi:10.7554/eLife.74094

Petit, I., Jin, D. and Rafii, S. (2007). The SDF-1-CXCR4 signaling pathway: a molecular hub modulating neo-angiogenesis. *Trends Immunol.* **28**, 299-307. doi:10.1016/j.it.2007.05.007

Shibata-Germanos, S., Goodman, J. R., Grieg, A., Trivedi, C. A., Benson, B. C., Foti, S. C., Faro, A., Castellan, R. F. P., Correra, R. M., Barber, M. et al. (2019). Structural and functional conservation of non-lumenized lymphatic endothelial cells in the mammalian leptomeninges. *Acta. Neuropathol.* **139**, 383-401. doi:10.1007/s00401-019-02091-z

Siekmann, A. F., Standley, C., Fogarty, K. E., Wolfe, S. A. and Lawson, N. D. (2009). Chemokine signaling guides regional patterning of the first embryonic artery. *Genes Dev.* **23**, 2272-2277. doi:10.1101/gad.1813509

van Impel, A., Zhao, Z., Hermkens, D. M., Roukens, M. G., Fischer, J. C., Peterson-Maduro, J., Duckers, H., Ober, E. A., Ingham, P. W. and Schulte-Merker, S. (2014). Divergence of zebrafish and mouse lymphatic cell fate specification pathways. *Development* **141**, 1228-1238. doi:10.1242/dev.105031

van Lessen, M., Shibata-Germanos, S., van Impel, A., Hawkins, T. A., Rihel, J. and Schulte-Merker, S. (2017). Intracellular uptake of macromolecules by brain

lymphatic endothelial cells during zebrafish embryonic development. *Elife* **6**, e25932. doi:10.7554/eLife.25932

Venero Galanternik, M., Castranova, D., Gore, A. V., Blewett, N. H., Jung, H. M., Stratman, A. N., Kirby, M. R., Iben, J., Miller, M. F., Kawakami, K. et al. (2017). A novel perivascular cell population in the zebrafish brain. *Elife* **6**, e24369. doi:10.7554/eLife.24369

Wang, Y., Huang, J., Li, Y. and Yang, G. Y. (2012). Roles of chemokine CXCL12 and its receptors in ischemic stroke. *Curr. Drug Targets* **13**, 166-172. doi:10.2174/138945012799201603

Xu, C., Hasan, S. S., Schmidt, I., Rocha, S. F., Pitulescu, M. E., Bussmann, J., Meyen, D., Raz, E., Adams, R. H. and Siekmann, A. F. (2014). Arteries are formed by vein-derived endothelial tip cells. *Nat. Commun.* **5**, 5758. doi:10.1038/ncomms6758

Yang, C., Han, X., Jiang, X., Lei, X., Bai, L. and Xu, F. (2016). Relation between C-X-C motif chemokine receptor 4 levels and the presence and extent of angiographic coronary collaterals in patients with chronic total coronary occlusion. *Am. J. Cardiol.* **118**, 1136-1143. doi:10.1016/j.amjcard.2016.07.020

Yang, Y., Wang, H., He, J., Shi, W., Jiang, Z., Gao, L., Jiang, Y., Ni, R., Yang, Q. and Luo, L. (2021). A single-cell-resolution fate map of endoderm reveals demarcation of pancreatic progenitors by cell cycle. *Proc. Natl. Acad. Sci. U. S. A.* **118**, e2025793118. doi:10.1073/pnas.2025793118

Yaniv, K., Isogai, S., Castranova, D., Dye, L., Hitomi, J. and Weinstein, B. M. (2006). Live imaging of lymphatic development in the zebrafish. *Nat. Med.* **12**, 711-716. doi:10.1038/nm1427

Zhan, Y., Huang, Y., Chen, J., Cao, Z., He, J., Zhang, J., Huang, H., Ruan, H., Luo, L. and Li, L. (2018). The caudal dorsal artery generates hematopoietic stem and progenitor cells via the endothelial-to-hematopoietic transition in zebrafish. *J. Genet. Genomics* **45**, 315-324. doi:10.1016/j.jgg.2018.02.010

Zheng, H., Fu, G., Dai, T. and Huang, H. (2007). Migration of endothelial progenitor cells mediated by stromal cell-derived factor-1alpha/CXCR4 via PI3K/Akt/eNOS signal transduction pathway. *J. Cardiovasc. Pharmacol.* **50**, 274-280. doi:10.1097/FJC.0b013e318093ec8f